An analytical model for granular jamming beams with applications in morphing aerostructures

J. David Brigido-González* , Steve G. Burrow†, and Benjamin K.S. Woods‡
University of Bristol, Department of Aerospace Engineering, Bristol, BS8 1TR, UK

Modern aircraft wings use discrete, flapped control surfaces that are simple and effective, but which create a significant drag and noise penalty when used. This research is working towards the replacement of these flaps with a continuous morphing device that can increase the aerodynamic performance and reduce noise emissions. However, the need to create smoothly morphing aerostructures presents a fundamental challenge in that the structures need to be stiff enough to resist aerodynamic and inertial loads while being flexible enough to change shape with minimal energy required. One way to address this competing set of constraints would be to use a material that is able to actively vary its stiffness. Such a device could be softened while morphing and then stiffened to hold its morphed shape. In this work, granular jamming is proposed as a mechanism for creating a material which can change stiffness from a liquid-like state to a solid-like state through the application of an applied pressure field which jams together the grains to stiffen an otherwise soft material. The basic concept of switchable stiffness for morphing aircraft has been shown in previous work. This paper introduces an analytical model to describe the bending dominated behaviour of granular jamming based morphing structures. Four-point bending experiments are performed to validate the model, and detailed strain fields from digital image correlation measurements are used to further elucidate the micro-mechanics. The experimental data was compared against predictions from the proposed model, where it was seen that while the model is able to capture the presence of different regimes of response, the overall stiffness and strength are overpredicted. Possible sources of discrepancy are highlighted and motivate future work.

I. Nomenclature

A	=	Cross-sectional area
b	=	Width
δ	=	Displacement
h	=	Height
I_{cr}	=	Cracked or splitting second moment of area
I_g	=	Gross second moment of area
K	=	Bulk modulus
M	=	Bending moment
M_{cr}	=	Cracked or splitting moment
M_f	=	Ultimate bending moment
P	=	Vacuum pressure
ϕ	=	curvature
σ_b	=	Stress in the bottom-most part
σ_t	=	Stress in the uppermost part
θ	=	Slope
V	=	Shear force

*PhD student, Bristol Composites Institute (ACCIS), Department of Aerospace Engineering, Queen's Building, University Walk, Bristol, BS8 1TR, UK, david.brigido@bristol.ac.uk

†Reader in Aircraft Systems, Department of Aerospace Engineering, Queen's Building, University Walk, Bristol, BS8 1TR, UK, Stephen.Burrow@bristol.ac.uk

‡Lecturer in Aerosopace Structures, Bristol Composites Institute (ACCIS), Department of Aerospace Engineering, Queen's Building, University Walk, Bristol, BS8 1TR, UK, ben.k.s.woods@ bristol.ac.uk

ε = Strain
Z = Section modulus

II. Introduction

A. Switchable stiffness FishBAC

Aircraft control surfaces (e.g. ailerons, rudders, elevators, etc.) and high-lift devices (e.g. flaps, slats, etc.) are designed to change the lifting distribution for flight control; however, most of those control surfaces are discrete. Discrete control surfaces have a gap or discontinuity between the leading edge and trailing edge of the airfoil. Discontinuities along the wing lead to an undesirable premature detachment of the boundary layer around the wing surface, and therefore to a substantial increase of drag and noise, see figure 1 [1]. On the other hand, avian wings do not have gaps or discontinuities along their wings, because they have flexible wings that can freely morph allowing to keep the boundary layer attached to the wing surface and therefore reducing drag, see figure 1. Furthermore, avian wings have inspired the development of some interesting morphing aerostructures [2]. Since then, scientists have tried to cover the gaps of discrete control surfaces by using flexible wings that allow changing the wing shape smoothly.

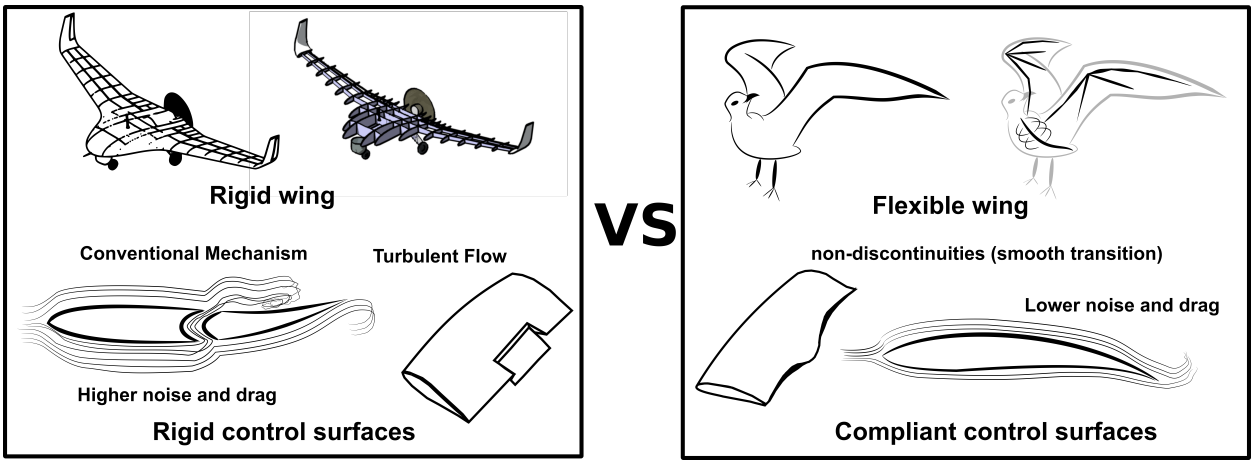

Fig. 1 Aircraft wings versus Avian wings

Flexible wings have also been used for load alleviation; that significantly reduces the weight [3]. Aeroelastic tuning for load alleviation can be improved with different techniques; probably the most successful ones are using composite materials to vary the flexural stiffness along the wingspan. For instance, the Grumman X-29 aeroplane has an un-balanced composite laminate that is used to generate the wash-out effect, which increased the divergence speed of the wing [4]. Recently the use of tow-steered composites, where the angles of the fibres are steered following path-following curves in the plane for each ply is an excellent technique to change the flexural stiffness along the wingspan [5]. The structural advantages of tow-steered composites over straight-fibre laminates are the increase of buckling loads, reducing the stress concentrations, etc. [6]. However, the most useful application is arguably aeroelastic tailoring. Stodieck et al., have proved that steering the fibres over the wing to achieve higher flutter divergence speeds, it can also alleviate gust loads or change the wing flight shape (morphing) by changing the flexural stiffness [7].

Aircraft structures have distinguishable substructures and components such as skin, panels, beams, mechanisms, actuators, etc. In contrast, Morphing structures aims to blur the distinction between those components by shifting conventional mechanisms or actuators, for smart materials and compliant mechanisms [8]. The improvement of aerodynamic performance by the use of morphing structures offsets the penalties associated with the additional weight and energy consumption. Butt [9] shows dramatic gains in performance using morphing aerostructures for different flight conditions (take off, cruise, manoeuvrings, etc.) of a military aeroplane over the traditional fixed-wing planes. His study concludes a decrease of 29% in fuel consumption and a 32% decrease in energy consumption over the same flight

mission using morphing structures.

The following research aims towards the efficient use of morphing aerostructures. The morphing device chosen for this work is the Fish Bone Active Camber (FishBAC) concept; which is inspired in part by the skeletal structure of fish, with an internal flexible spine allowing for large, continuous changes in camber and also supporting a flexible skin [10]. The FishBAC has an embedded servomechanism with a pulley that is connected through the flexible spine to deflect the camber (see picture 2). Rivero et al., have been working on varying the flexural stiffness of the FishBAC by using composites layups along the spine. The flexural stiffness of the camber can be tuned if different stacking sequence layups are being used; which can significantly affect the torque required for the actuator to withstand the aerodynamic loads [11].

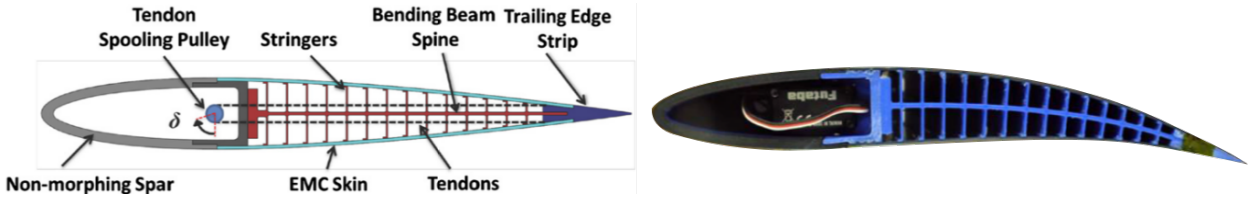

Fig. 2 The Fish Bone Active Camber (FishBAC) Concept. Pictures taken from [12–14].

The key underlying concept of this research is to incorporate an active stiffness material into the structure of the FishBAC, to allow it to soften during actuation/morphing and to then stiffen once in the desired shape to reduce the actuation effort required to maintain shape. This active stiffness material is based on the principle of granular jamming, where granular material (sand, glass beads, coffee grains, etc.) are contained within an airtight membrane to form a structural element. This element has very low stiffness in its nominal state, as the grains are able to flow and slide over each other. When vacuum is applied within the membrane; however, the air is removed, and the resulting atmospheric pressure compresses the grains together to create a locked, stiffened structure. This basic principle can create a significant change in the resulting stiffness of a morphing structure such as the FishBAC. Initial prototypes of this concept showed that the granular jamming media allows for real-time control of the bending stiffness of the FishBAC [15]. It is also capable of switching the stiffness to withstand the aerodynamic loads without requiring power from the actuator. The efficiently manage of vacuum pressure during actuation and holding can significantly reduce the actuation torque and energy consumption. For example, it is possible to provide a zero-energy consumption, if the actuator is switch off during holding position because the shape is maintained due to granular jamming. The combination of these two concepts (FishBAC and granular jamming) shows the development of a new morphing concept known as Switchable stiffness FishBAC (SwitchBAC) [15], and is shown schematically in Fig. 3.

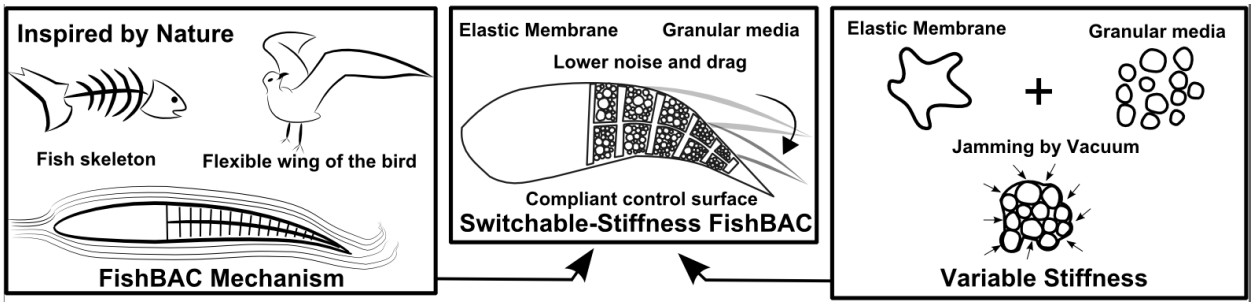

Fig. 3 SwitchBAC Concept. Pictures taken from [15]

The skeleton structure of the FishBAC was 3D printed in polylactic acid. It has 12 chambers (6 in the upper camber and 6 in the lower camber) composed between the stringers of the FishBAC, and are filled with coffee grains due to its weight/stiffness relation. The chambers are enclosed in a silicone membrane glued on top of the stringers to build numerous sealed chambers along the spine. The vacuum flux passes through the chambers, which are linked

by opening channels in the stringers; however, the slots had filters to stop the passage of the granular material. In this way, the vacuum sucks the air inside the cavities, leading to jamming the grains under the external atmospheric pressure. Thus, the bending stiffness along the spine can be tuned in real time by varying the vacuum pressure. Fig. 4 shows the SwitchBAC concept and the flexural tests using a test frame machine. The figure shows the results of the load-displacement curves for different vacuum levels. It can be seen that the stiffness increases as the vacuum level rises. The morphing device can switch stiffness more than 250% with respect to no-jamming stiffness (only the spine stiffness).

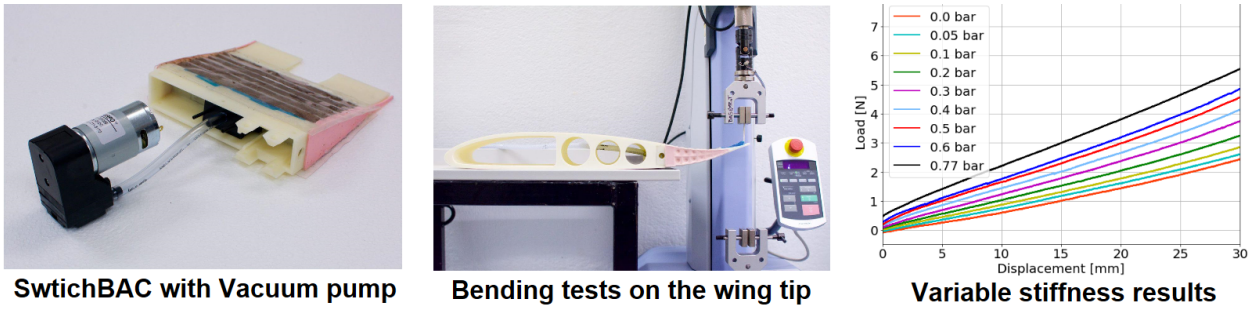

Fig. 4 SwitchBAC connected to a vacuum pump (a), SwitchBAC bending tests (b), Variable stiffness results (C). Pictures taken from [15]

Nevertheless, the SwitchBAC has another useful feature; it can be actuated by differential changes of vacuum pressure between the upper and lower chambers. If there is a differential pressure above and below the spine, there would be bending moments that would deflect and actuated the camber. For instance, the spine can be deflected upwards if there is a more significant vacuum pressure on top than bellow (see Fig. 5 picture b); conversely, the spine can be deflected downwards for a bigger pressure on the lower chambers (see Fig. 5 picture c).

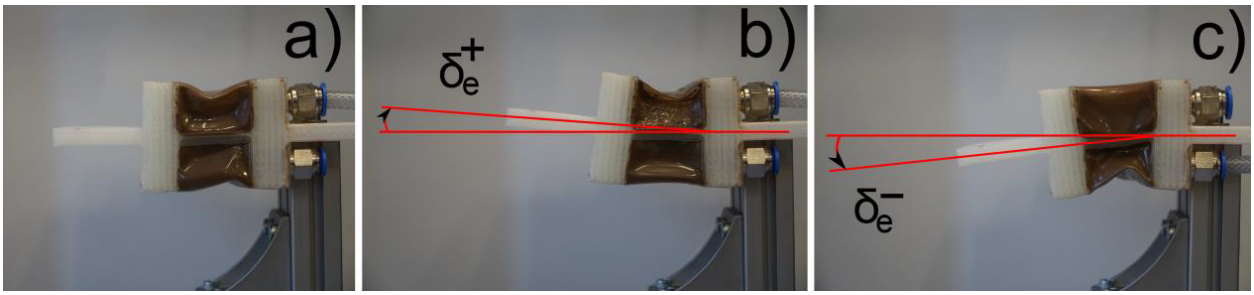

Fig. 5 No spline deflection (a), upwards spine deflection (b), downwards spine deflection(C). Pictures taken from [15]

B. Granular jamming

Granular media can be jammed by controlling the packing fraction volume, known as ϕ. This parameter is the dimensionless relationship of the volume of the whole structure concerning the volume of all the particles. The following equation describes this dimensionless relationship.

$$\phi = \frac{\sum N_p V_p}{V_s} \tag{1}$$

where N_p is the number of particles in the structure, V_p is the volume of all the particles, and V_s is the volume of the structure. Granular jamming systems can have different packing volume properties and different types of contacts among particles. Liu and Nagel designed a useful diagram used to describe jamming in granular materials [16]. The

Fig. 6 left picture shows how a granular media system can change from an unjammed state to a jammed state by varying shear stress and packing fraction; which is delimited by the isotropic jamming point or J point. The jamming occurs when the density rises, and the J point can be found precisely when the particles slightly touch each other, but the pressure is still zero. Otherwise, when the pressure is different from zero, the system jams. The volume change can be measured with the following relationship: $\Delta\phi = \phi_j - \phi$ where ϕ_j is the critical density located at J point. The variation of behaviour (from fluid-like to liquid-like and vice versa) is represented as the variation between the bulk and shear modulus. The Bulk or compression modulus represents how resistant a disordered or ordered package is for a homogeneous compression [17]. On the other hand, the shear elastic modulus is the resistance of packing to pure shear. The J point can predict the relation between the bulk K and shear G modulus, and relate the transition from solid-like state to liquid-like state and vice-versa [18]. In a critical-stable condition, it is possible to relate the following restriction $\Delta\phi = -\phi_j + \phi > 0$. Nevertheless, the relation $K = G$ is marginally stable or jammed state above ϕ_j. This state is quite sensitive to shear than compression; it behaves like a fluid in case that $\Delta\phi$ is drawing near to zero. On the other hand, if $\Delta\phi$ increases, the $K = G$ relationship decreases, and the aggregate material behave like a solid (The Jammed states are confined to a region of low shear stress and high density) [19]. Further increment in ϕ, allows the whole system to resist larger shear stresses before the system becomes unstable and unjammed.

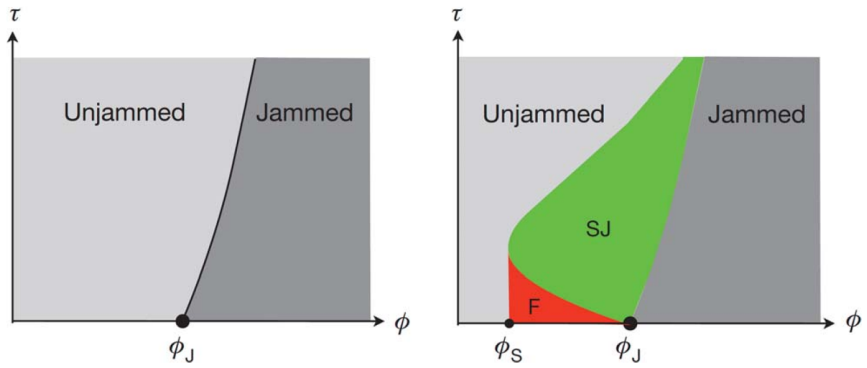

Fig. 6 Jamming state transition for smooth (left) and frictional (right) material. Pictures taken from [16]

The variation of stiffness for granular jamming devices can be tuned (variation of shear stress due to variation of contacts) if an external stimulus controls the volume change. There are different ways to control the volume change; one way is to contain the granular media inside of an airtight membrane and to use vacuum pressure to control packing fraction. Pulling a vacuum inside the membrane removes the air between particles and the resulting external atmospheric pressure compresses the media - decreasing the volume of material within the membrane (increasing packing fraction) and applying a compressive force to the media, increasing the shear stresses between particles. Varying the extent to which vacuum is pulled varies the internal air pressure, and therefore the net pressure across the membrane, allowing for proportional control of packing fraction and applied stresses. Granular jamming devices that are composed of grains inside an elastic envelope controlled by a vacuum pump are sometimes known as 'Vacuumatics' or 'Deflateables'. Such devices have been used to create architectural, robotic, and civil engineering structures, but to date have not been applied to morphing aircraft concepts. One early example of a granular jamming bases structure was the dome structure presented in [20], which was built of Expanded Polystyrene beads within a polymer membrane. The main objective of this work was to demonstrate a concept for reconfigurable buildings.

Another common area of application for granular jamming based structures is in robotics and medical devices. For example, the Vacu-SL is a granular jamming based variable stiffness catheter [21]; it uses glass beads as the granular media, contained in an elastomeric membrane. The granular jamming device can switch stiffness for different stages of the implanting procedure; to better balance between the conflicting requirements of softness for interaction with the patient (and injury avoidance) versus stiffness for positional accuracy and control. Granular jamming structures have also been proposed for soft robotics applications, particularly bending dominated applications. A significant body of previous research has explored different aspects of this application area. Cheng et al. [22] propose a design methodology for granular jamming based soft robotic arms, and use triaxial compression tests to quantify the response of a series of different grain types under vacuum pressure. Huijben et al., [23] considered the flexural response of such

devices using four point-bending tests and also developed numerical models using DEM (Discrete element method) and FEA (Finite Element Analysis) techniques. The load-displacement curves taken from the experimental data show a highly non-linear behaviour. The complex response of the granular media under bending is still poorly understood, and more experimental, and modelling effort is needed to get to the point where variable stiffness structures can be designed which accurately incorporate the complex non-linear response of the granular media under varying levels of vacuum pressure and applied loading .

In previous work by these authors, have also tested granular jamming beams in four-point bending to obtain the non-linear stress-strain curves. The stress-strain curves are used on a non-linear FEA model based on Von-Mises plasticity to obtain the flexural stiffness. The previous approach is a useful approach to predict the variation of stiffness of granular jamming beams in a simplified way, and within the constraints of Euler-Bernoulli beam bending assumptions [15]. However; a more generally applicable modelling of the complex, non-linear micro-mechanical response of granular jamming bending structures is needed, which motivates the combined experimental and analytical approach pursued here.

The following sections propose a new analytical method for granular jamming beams that is informed by previous analysis work in soil mechanics and inflatable beams. First, the physics on bending for prestressed concrete beams are explained, focusing on the decreasing of the second moment of area due to crack propagation. The flexural physics on prestressed concrete beams motived a similar explanation for granular jamming, instead of the crack propagation, there is a sliding of particles. Second, four-point bending tests using Digital Image Correlation techniques (DIC) shown how the beam shrinks due to particle sliding. Once that the change of moment of area is bear out using DIC, then an analytical model is proposed following that principle. Finally, the model results are compared with experimental data.

III. Flexural properties in granular jamming beams

Concrete structures such as bridges that are analyzed as beams under structural loading, the granular material cannot withstand tensile stress. However, concrete beams crack under tension, losing its flexural strength [24]. Fig. 7 shows a simply supported beam subjected to a distributed uniform load due to self-weight and a point load. The moment distribution is parabolic and increases all the way through the mid-span. In the uncracked section, the stress-strain distribution is considered to be fully functional, and the entire cross-section is contributing to the bending resistance, as a result of that, the second moment of area has not suffered any particular change. As the bending moment increases towards the midspan, the bottom particles of the cross-section start to separate, this is known as the cracking moment. The crack grows from the bottom section, and the neutral axis shifts upwards; therefore, the second moment of area decreases. The section that is cracked is not contributing to the flexural stiffness of the beam; only the compression strength above the neutral axis is sustaining the stress [25].

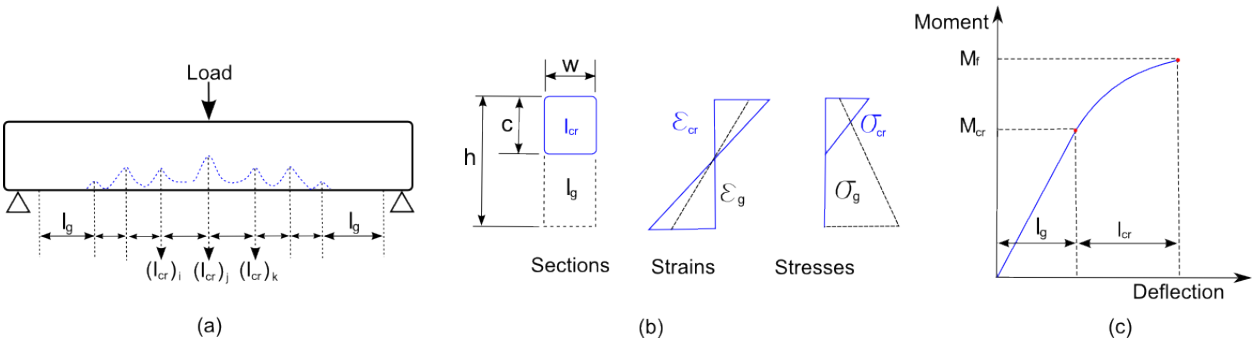

Fig. 7 a) Change of second moment of area, b) strains and stress of a concrete beam, c) cracking moment.

Beams with reinforcement or pre-stressed beams can support tensile loads. Reinforcement beams use steel rods located below the neutral axis, with the objective that the rods support the tensile stresses. Pre-stressed beams often have an asymmetric axial pre-force that moves the neutral axis downwards, which increases the portion of the cross-section area that is in compression and decreases the section in tension, an advantageous design feature for materials with

limited tensile strength [26].

Granular media, like concrete, have poor tensile strength and so granular jammed structures can take advantage of the pre-stressing concept. In this case, the pre-stressing comes from the vacuum pressure, which acts overall external faces of the structure to create a pre-compression stress in the media, which partially offsets tensile stresses induced by bending. As the bending loading increases, the structure will reach a critical loading point where the tensile stresses from bending just overcome the pre-compression in certain areas of the structure, and at this point the grains on the face of the tensile surface will begin to split (see Fig. 8), and will no longer be able to carry load. As load is increased further still, there will be a progressive movement of this splitting point inwards through the thickness, and an increasing portion of the span of the beam will become ineffective. This leads to a progressive reduction in the effective second moment of area of the beam, which induces a softening response, as shown experimentally in previous work by these authors [15].

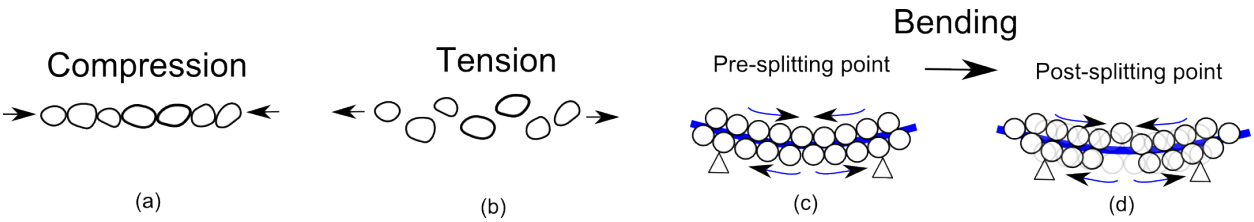

Fig. 8 a) axial force due to vacuum, b) splitting force due to tensile force, c) pre-splitting point due to bending, d) post-splitting point due to bending.

A series of rectangular cross-section beams were built using an elastic membrane and granular material as the core, with dimensions of 120mm wide, 40mm high and 600mm long. Huijben analyzed glass spheres of different sizes using flexural tests and showed that the difference of this parameter does not affect the flexural stiffness of the beam [23]. His research also showed that the variation of stiffness changes drastically for each type of granular material [23]. In this work, it was characterized not only the type of material but also the shape. Materials with two different shapes (spherical, irregular) were selected with similar sizes in order to demonstrate the variation between them. At the same time, a mix between them (hybrid grains) was also analysed. For smooth material, glass beads were used. For irregular material and with a similar weight to the glass, sand was chosen, and coffee was chosen because previous research has shown it to have a high strength to weight ratio as a granular media [22]. In Fig. 9 c) can be seen the three types of materials used. The hybrid combinations of materials consisted of all three permutations (glass/sand, coffee/glass, coffee/sand) of carefully mixed 50%/50% mixtures by volume.

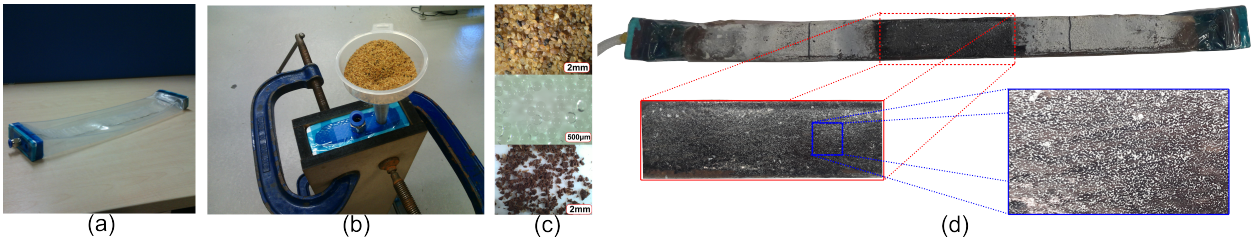

Fig. 9 a) elastic membrane, b) sample preparation, c) granular materials, d) speckle pattern for DIC

For the vacuum containment membrane, a 0.5mm thick silicone sheet was chosen due to its high strain capability and low stiffness. To maintain the rectangular shape of the beam, the skin was wrapped around and bonded to rectangular end-fittings. In one of the end-fittings, two holes were made, one for filling the grains and one for a vacuum fitting. The vacuum port was insulated from the grains with a porous fabric to allow for air flow while keeping the grains inside the beam. Fig. 9 a) displays the silicone sheet membrane with end-fittings.

To maintain geometric consistency and experimental repeatability, a rectangular female mould was used to set the shape of the beam. The filled specimen was placed inside this mould while at atmospheric pressure such that it took the

desired rectangular shape. Vacuum was then applied to jam the beam into this shape, and the beam was then removed from the mould and placed on the four-point bending test rig.

Four-point bending tests were performed using a test frame machine with a load cell of 1kN. The bending tests followed the ASTM C880/C88M21 standard. The curvature and strains values were taken using a video gauge system and Digital Image Correlation techniques (see Fig. 10).At least eight tests were run on each combination of material and vacuum level. Three vacuum levels were tested: 0.5 bar, 0.75 bar, and 1 bar.

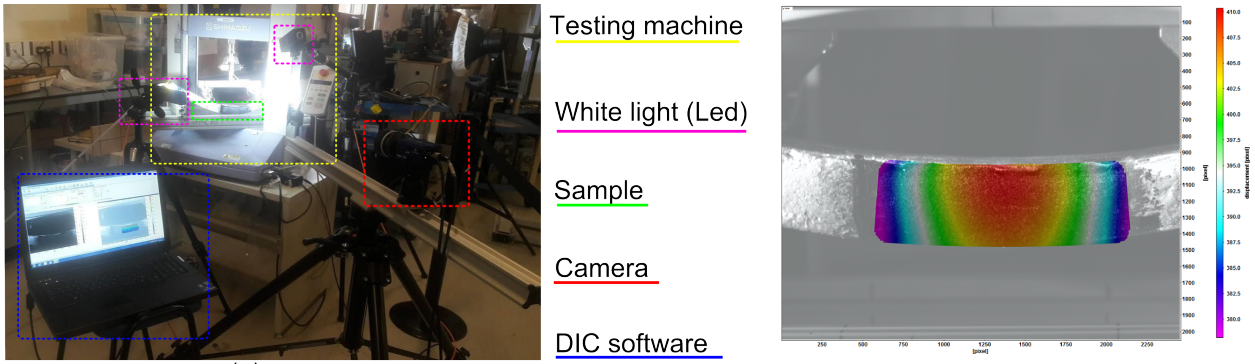

Fig. 10 a) test setup, b) full-field of the displacement using DIC

On the other hand, it is known in the literature that the flexural stiffness and transverse strain distribution of a prestressed concrete beam are linear before the cracking moment, but once the cracking moment has been reached, the stiffness and transverse strains become non-linear due to decreasing of the second moment of area [27]. This work undertook the first detailed strain measurements of granular jammed bending beams in the literature in order to better understand the detailed mechanics of the complex non-linear bending responce of these structures. The main objective of performing flexural tests using DIC is the interest of knowing whether the transverse strain distribution varies significantly with increasing load.

The full-field axial and transverse strains using DIC are shown in Fig. 11 and Fig. 12. The axial strain distribution results remains linear despite overcoming the splitting moment. The previously axial strains results show a similar lineal strain distribution behaviour than experimental tests results using concrete beams [28]. In Fig. 12 can be seen that the transversal strains decrease in a non-linear manner. The changes in deformation indicate that what is below the neutral axis contracts; while the local thickness of the beam expands above the neutral axis. This is due to motion of the grains under compressive loading, which induces sliding in the grains (once a critical load is reach), forcing the grains outwards and generating a local increase in thickness. The DIC system can only show the deformation of the membrane and not the slippage of the grains, it is speculated that shrinkage is due to the splitting moment separating the particles that are at the bottom of the section; this phenomenon can also be appreciated in Discrete Element Methods simulations (DEM). DEM have shown the sliding and separation of the particles in the lower part; and the compression and push upwards of particles in the upper part of granular jamming beams subjected to bending loads [23, 29].

IV. Proposed Model for granular jamming beams

Fig.13 shows a granular jamming beam with a prestress force due to vacuum p submitted to three different conditions of bending load. An arbitrary loading for the following beam is expressed by applied moments that are functions of the longitudinal beam coordinate x. A model of a granular jamming beam submitted to vacuum must accommodate the splitting region (see Fig.13(c)) as defined previously, and the normal operation regions (see Fig.13(a) and (b)). The stress distribution for all the bending conditions illustrated in Fig.13 are assumed.

Firstly, In the normal operation region (before the splitting region), the stress distribution in the outermost (top and bottom) part of the beam can be calculated in the following way.

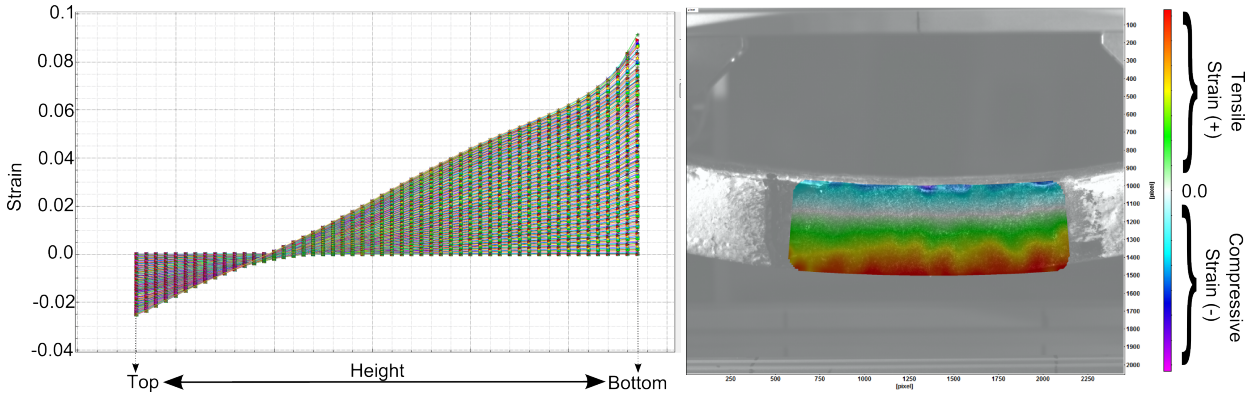

Fig. 11 Full-field of the axial strain using DIC

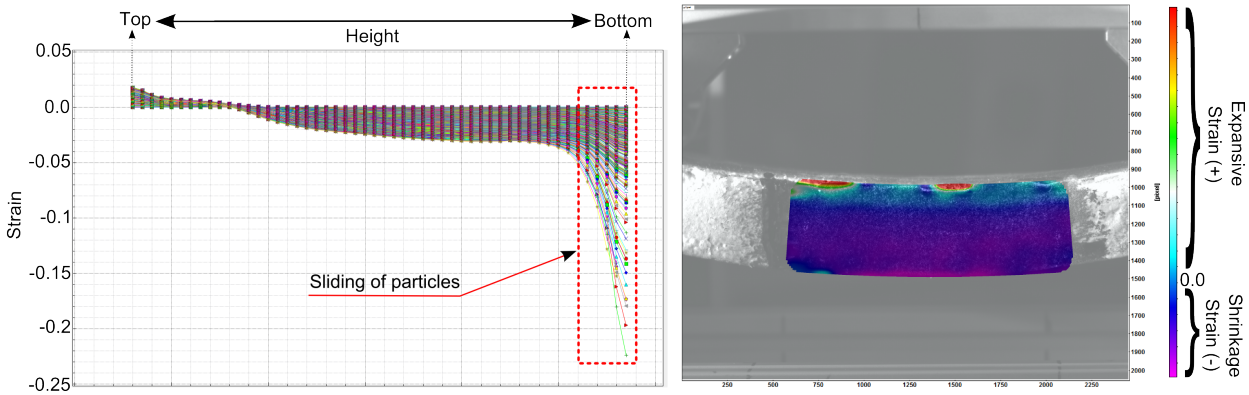

Fig. 12 Full-field of the transversal strain using DIC

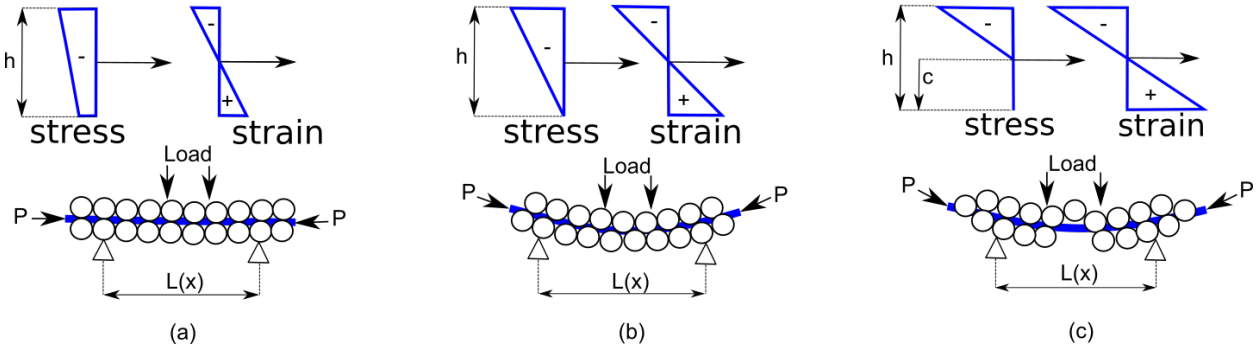

Fig. 13 Stress and strain distributions for normal operation region (a), decompression region (b) and splitting region (c)

$$\sigma_t = -p - \frac{M}{Z} \tag{2}$$

$$\sigma_b = -p + \frac{M}{Z} \tag{3}$$

Where p is the axial prestress due to vacuum, M is the bending moment due to self weight plus active load, Z is the section modulus, and A is the cross-sectional area. The cross sectional area and section modulus for a rectangular cross-sectional shape beam are:

$$Z = \frac{wh^2}{6} \tag{4}$$

$$A = wh \tag{5}$$

where w is the width of the cross-section and h is the height. Because the axial stresses are compressive (for small values of bending moment), it is easy to calculate the curvature of the beam using Euler-beam approach; the following equation calculates the curvature of the beam for the normal operation region.

$$\phi = \frac{\varepsilon_t - \varepsilon_b}{h} \tag{6}$$

where ϕ is the curvature, ε_t is the strain in the top section of the beam, and ε_b is the strain in the bottom section of the cross-section. The stress distribution is linear along with the height of the cross-section; thus, the stresses in the outermost part can be substituted for strains using the Hooke's stress-strain relation. Substituting the strains relation from Eq. 6 into Eqs. 3 and 2, the curvature is equal to the Euler-Bernoulli's equation for flexural stiffness calculation.

$$\phi = \frac{M}{EI} \tag{7}$$

where EI is the flexural stiffness. As can be seen in the following equations, the axial stress due to vacuum does not contribute at all into the flexural stiffness. Assuming, that the stiffness is a linear variation of the pressure, it is possible to account this phenomenon using the following force diagram (see Fig.14) for an infinitesimal element of the beam and the following behaviour laws:

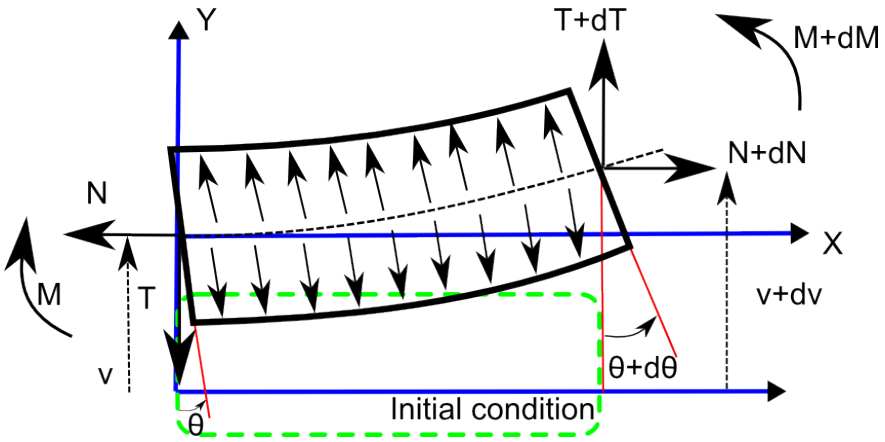

Fig. 14 Force diagram for an infinitesimal element

$$N = N_0 = p \tag{8}$$

$$T = kGA(\frac{\mathrm{d}}{\mathrm{d}x}V - \theta) \tag{9}$$

$$M = EI\frac{\mathrm{d}}{\mathrm{d}x}\theta \tag{10}$$

The first equation is the axial force, and the second and third equation describes the shear and moment. The shear is account assuming Timoshenko's approach, where G is the shear modulus, and k is the shear correction factor. From the force diagram, the following equilibrium equations can be calculated.

$$\frac{\mathrm{d}}{\mathrm{d}x}N_0 = 0 \tag{11}$$

$$\frac{\mathrm{d}}{\mathrm{d}x}(\frac{\mathrm{d}}{\mathrm{d}x}V - \theta)(p + kGA) = 0 \tag{12}$$

$$-(\frac{\mathrm{d}}{\mathrm{d}x}V - \theta)(p + kGA) - (E + \frac{p}{A})I\frac{\mathrm{d}^2}{\mathrm{d}x^2}\theta = 0 \tag{13}$$

An analytical solution can be obtained using the boundary conditions of a cantilever beam. The Eqs. 14 and 15 show the slope and displacement for a cantilever beam with an active punctual load at the end tip.

$$\theta(x) = \frac{F}{EI + pI/A}(\frac{x^2}{2} - Lx) \tag{14}$$

$$\delta(x) = \frac{F}{EI + pI/A}(\frac{x^3}{6} - \frac{Lx^2}{2}) - \frac{Fx}{p + kGA} \tag{15}$$

The previous equations account for the variation of pressure in the bending stiffness and the shear stiffness. The deflection is still a linear function of the applied load or bending moment. As the applied load increases beyond the critical load, the splitting point moves upward through the beam and the inactive region below the splitting point grows in size in both the thickness and axial directions. The splitting bending moment can be calculated by setting Eq. 3 to zero. Eqs. 16 and 17 show the splitting point condition; and the stress distribution for the splitting region is illustrated in Fig. 13 (c).

$$\sigma_b = -P + \frac{M_{cr}}{Z} = 0 \tag{16}$$

$$M_{cr} = ZP \tag{17}$$

The stress resultant in the axial direction can be calculated using a linear function of the total stress in the outermost part of the beam.

$$\sigma = \frac{\sigma_t y}{h/2 - C} - \frac{\sigma_t c}{h/2 - C} \tag{18}$$

Where σ_t is the total stress in the outermost part of the beam, C is the portion of the beam's thickness that is contributing to the stiffness, and it varies as the second moment of area is changing due to an increase of bending moment.

The following equation relates the sum of moments about the transverse axis through the centre of the beam.

$$M = -\int_c^{h/2}(\sigma w y)\,\mathrm{d}y = \frac{(C + h)(-h + 2C)w\sigma_t}{12} \tag{19}$$

Isolating σ_t from the previous equation leads to the following relation.

$$\sigma_t = \frac{12M}{(C + h)(-h + 2C)w} \tag{20}$$

Then, a sum of axial forces is obtained in the following equation.

$$F = -\int_c^{h/2}(\sigma w)\,\mathrm{d}y = -\frac{(-h + 2C)w\sigma_t}{4} \tag{21}$$

Again, isolating σ_t from the last equation leads to the following equation:

$$\sigma_t = -\frac{4Ph}{-h + 2C} \tag{22}$$

Solving and equating σ_t expressions in Eqs. 20 and 22, yields to the calculation of distance C as a function of the bending moment and pressure.

$$C = \frac{3M}{Pwh} - h \tag{23}$$

As mentioned before, the non-linear region which occurs after the splitting point is driven primarily by the reduction in the second moment of area due to an increasing portion of the beam no longer carrying load. Thus, the beam curvature in Eq. 7 changes to Eq. 24. Fig. 15 explains the change of curvature from a normal operation to a splitting region.

$$\phi = \frac{\varepsilon_t}{c} = \frac{M}{EI_{cr}} \tag{24}$$

$$I_{cr} = \frac{w((C + h)(2C - h)^2)}{24} \tag{25}$$

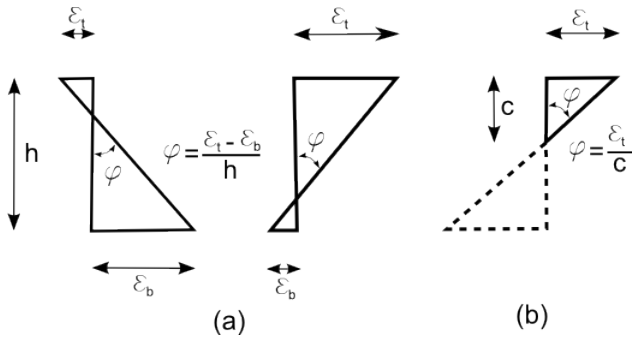

Fig. 15 Curvature for normal operation region (a) and splitting region (b)

Equation 25 relates the change of the second moment of area with respect to the height of the beam. Fig. 16 plots this relationship and the distance C shows the section of the beam that is only capable of sustain compressive load as the bending moment increases or the second moment of area decreases. The plot shows that the decreasing value of the second moment of area follows a non-linear behaviour as the distance C increases. The curvature of the beam achieves its maximum load-carrying capacity when the distance C is equal to half of the height of the cross-section (the last section of the beam that can sustain compressive loads). The maximum bending moment that can withstand the structure before failing is shown in Eq. 27.

$$C = \frac{3M_f}{wph} - h = \frac{h}{2} \tag{26}$$

$$M_f = \frac{pwh^2}{2} \tag{27}$$

Fig. 16(b) shows that the bending moment remain linear before the splitting point, but once that point is overcome, the non-linear behaviour appears due to decreasing of the second moment of area. The following step is to compare the new model with respect to the experimental data taken from the four-point bending test. The flexural stiffness of a granular beam considering self-weight can be known if the shear force and bending moment can be calculated in function of the active load, and the distributed load (self-weight). The shear force and bending moment diagrams for a four-point bending beam are shown in Fig.17a. Knowing the stress-strain relations, and flexural stiffness for the normal

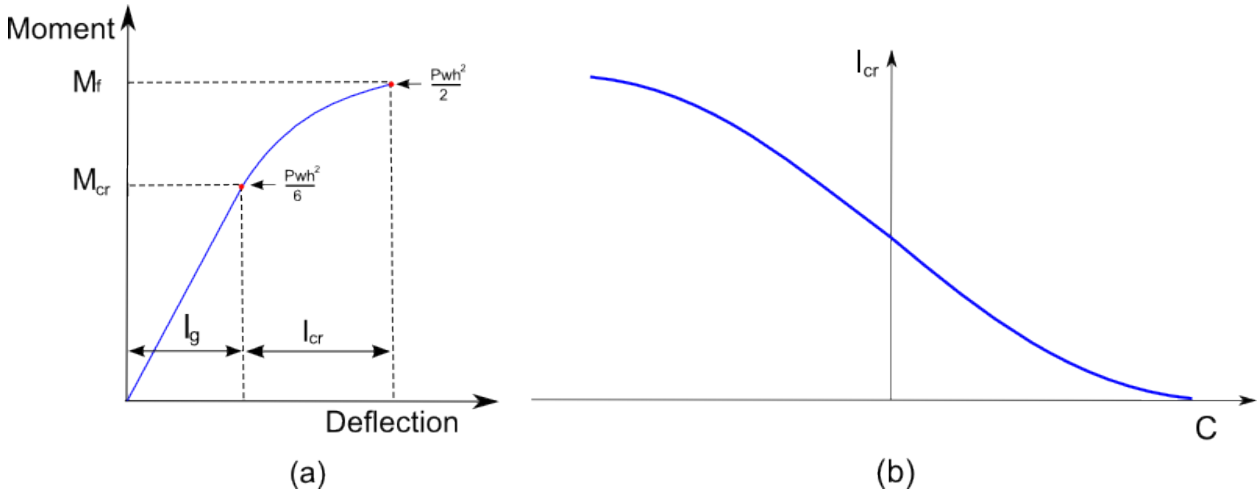

Fig. 16 Non-linear behaviour for a flexural beam due to change of second moment of area

operation and splitting regions, it is possible to calculate the slope and the deflection of the beam. The main goal of this research is to compare the proposed model against the experimental results from the four-point bending tests. Fig 17b shows the experimental load-displacement curves for coffee grains with a vacuum variation of 0.5, 0.75 and 0.85 bar.

The first derivative of the slope and the displacement can be numerically integrated for any given non-uniform bending moment (M) and flexural stiffness (EI). All the steps for the length of the beam are defined at a suitable number of discrete locations $x_0, x_1 ..... x_i ..... x_{n-1}, x_n$. The differential equations can then be approximated over the interval $x_i .....x_{i+1}$ via averages and finite differences. The numerical integration was done using the trapezoidal rule. The statically determinate beam can be discretely integrated if the boundary conditions are taken into account and following the right order of the sums. The boundary condition for the slope starts at the half of the length; then the sum values are summed from the half to the root. The boundary condition for the deflection starts at the root; therefore, the sum values are summed from the root to the half of the length once the numerical integration of the slope was done before. The following equations show the boundary conditions and numerical integration for the slope and the deflection.

$$x = \frac{L}{2} ..... \theta_0 = 0 \tag{28}$$

$$x = 0 ..... \delta_0 = 0 \tag{29}$$

$$T_i = V_{i-1} + \frac{V_i + V_{i-1}}{2}(x_i - x_{i-1}) \tag{30}$$

$$\theta_i = \theta_{i+1} - \frac{1}{2}\left(\frac{M_{i+1}}{EI_{i+1}} + \frac{M_i}{EI_i}\right)(x_{i+1} - x_i) \tag{31}$$

$$\delta_i = \delta_{i-1} + \frac{\theta_i + \theta_{i-1}}{2}(x_i - x_{i-1}) + T_i \tag{32}$$

The numerical results are shown in Fig 18 and 19. The model has dimensional and mechanical parameters as an input, for instance, the height of the beam, cross-sectional area, young modulus, shear modulus, etc. However, the stiffness parameters are the most important, and these values can be approximated from the experimental data of the four-point bending tests. For the following model, the young modulus was taken from the flexural-stiffness of the coffee grains beams, and the shear modulus was taken from shear-tests made by Cheng et al [22]. The Fig 18a displays that the splitting point is highly sensitive to the young modulus. The splitting point is shown early for lower values of young modulus. The graph shows a comparison between young modulus of 10 Mpa against 2.5 Mpa. Besides, Fig 18b indicates that the flexural stiffness is also sensitive to shear modulus, and it displays the stiffness variation for a model that considers shear deformation, in contrast to a model that does not consider the Timoshenko approach.

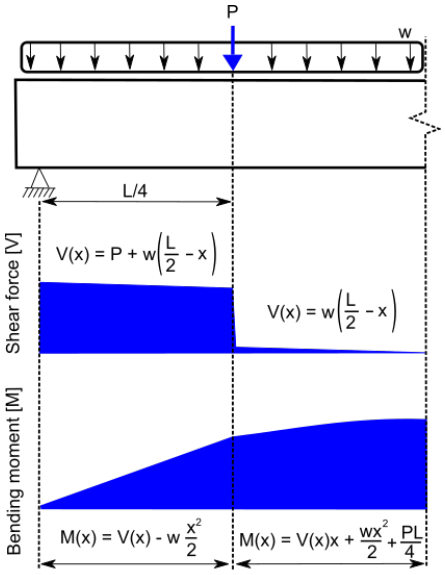

(a) Shear force and bending moment diagrams

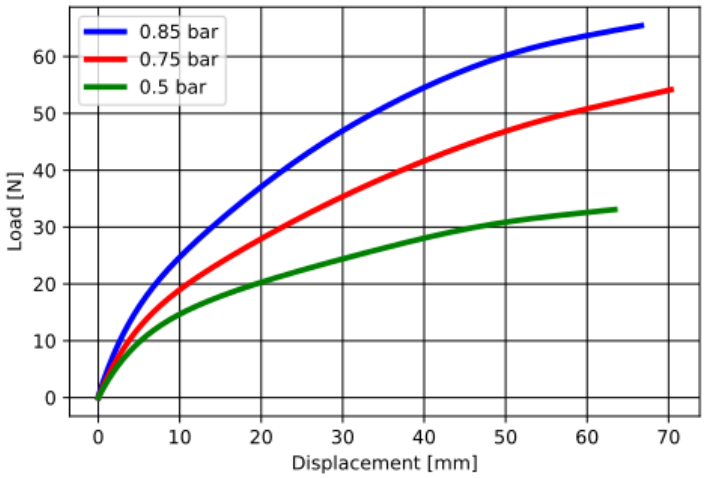

(b) Experimental results for coffee grains

Fig. 17 Four-point bending

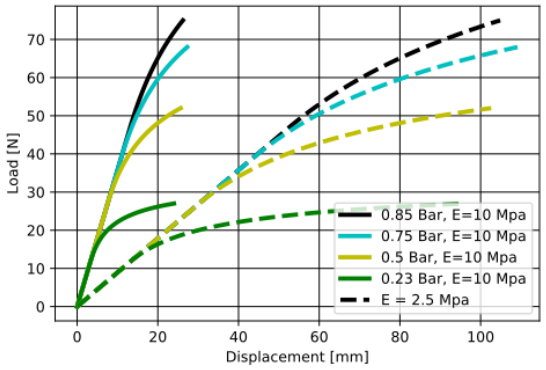

(a) Elastic modulus variation

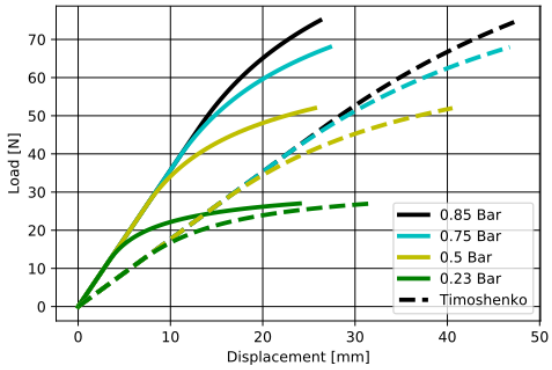

(b) Shear modulus variation

Fig. 18 Variation of parameters for the proposed model

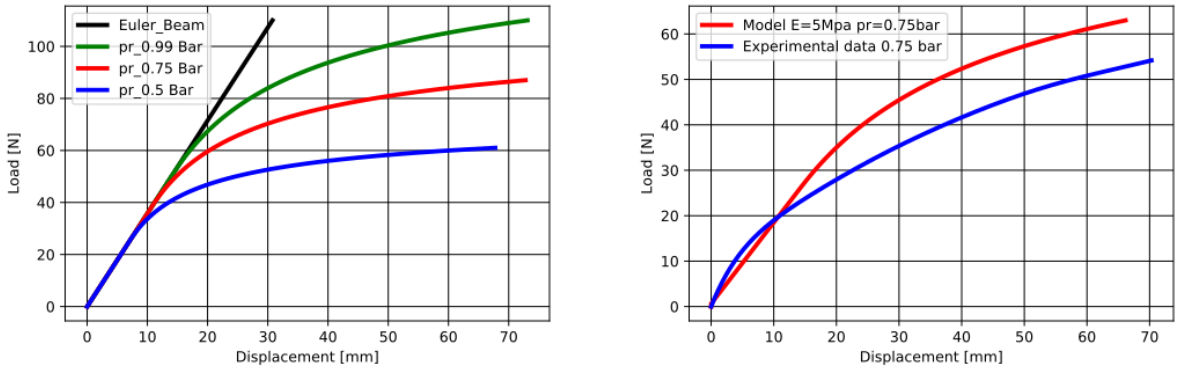

(a) Euler beam comparison **(b) Experimental data comparison**

Fig. 19 Numerical results of the proposed model

Nevertheless, Fig. 19a, shows the comparison of the new model at different vacuum pressures with respect to the Euler beam approach. The Euler-beam approach does not take into account the non-linear behaviour because it does not account the change of the second moment of area. But the model proposed can capture the non-linear behaviour due to change of the second moment of area, and the graph displays that the splitting region can be delayed as the vacuum pressure increases.

Fig. 19b shows the comparison between the experimental data and the model. This comparison is for granular coffee at a vacuum pressure of 0.75 bar. It can be seen, that the model follows the same trend that the experimental data; however, the splitting point of the experimental is shown earlier than the model (10% error). It is speculated that the stiffness difference is due to the fact that some physical phenomena are ignored. One of the possible improvements is to take into account the mechanics of grains. Grain mechanics is highly driven by shear strength, which accounts for the interlocking effect between particles due to friction and cohesive forces.

V. Conclusions and future work

This work presents progress towards the goal of a switchable stiffness material for use in morphing aircraft structures. In order to quantify the detailed micromechanics of how the granular media jams and strains during the course of large displacements in a 4 point bending test, DIC on the outer side skin surface was used to track strains. Both directions of in-plane strain were tracked. An analytical model of the material behaviour is developed, which captures key physical behaviour immediately, and detailed experiments highlight critical details of the granular media micro-mechanics which should be considered in future iterations of the model.
Several key conclusions can be drawn from each phase of this research in the following list:

- The longitudinal strains show non-linear gradients of strain through the thickness, highlighting the splitting effects. Furthermore, through-thickness strains show a local thinning of the beam in the splitting region and a thickening of the beam in the upper compression surface.
- A new modified version of Euler's beam theory was proposed. This new formulation is inspired by the analysis of inflated structures and prestressed concrete beams.
- The model is highly sensitive to young and shear modulus inputs. Where it can be approximated them using experimental bending and shear tests in order to calculate the bulk and shear modulus.
- The proposed model takes into account the axial stress distribution due to the vacuum, and it captures the non-linear behaviour due to the splitting point; however, the model needs further improvement. As future work, the model should consider the micro-mechanics of the grain.

Acknowledgments

The research was funded in part by the Engineering and Physical Sciences Research Council through the EPSRC Centre for Doctoral Training in Advanced Composites for Innovation and Science(grant number 1791399) with further support provided by the European Research Council (ERC) under the European Union's Horizon 2020 research and innovation programme, as part of the Shape Adaptive Blades for Rotorcraft Efficiency (SABRE) programme (grant agreement No 723491). The authors would like to acknowledge the help of Marco Longana, the Aero-ACCIS lab support and CONACYT (the National Council of Science and Technology).

References

[1] Glauert, H., *The elements of aerofoil and airscrew theory*, Cambridge University Press, 1983.

[2] MacCready, P. B., "Of birds, bees, and airplanes: Technology can take lessons from nature on how to produce flying machines," *IEEE Potentials*, Vol. 6, No. 2, 1987, pp. 29–32.

[3] Cook, R. G., Palacios, R., and Goulart, P., "Robust gust alleviation and stabilization of very flexible aircraft," *AIAA journal*, Vol. 51, No. 2, 2013, pp. 330–340.

[4] WEISSHAAR, T., "Aeroelastic tailoring-Creative uses of unusual materials," *28th Structures, Structural Dynamics and Materials Conference*, 1987, p. 976.

[5] Gurdal, Z., and Olmedo, R., "In-plane response of laminates with spatially varying fiber orientations-variable stiffness concept," *AIAA journal*, Vol. 31, No. 4, 1993, pp. 751–758.

[6] Kim, B. C., Potter, K., and Weaver, P. M., "Continuous tow shearing for manufacturing variable angle tow composites," *Composites Part A: Applied Science and Manufacturing*, Vol. 43, No. 8, 2012, pp. 1347–1356.

[7] Stodieck, O., Cooper, J. E., Weaver, P. M., and Kealy, P., "Improved aeroelastic tailoring using tow-steered composites," *Composite Structures*, Vol. 106, 2013, pp. 703–715.

[8] Vasista, S., Tong, L., and Wong, K., "Realization of morphing wings: a multidisciplinary challenge," *Journal of aircraft*, Vol. 49, No. 1, 2012, pp. 11–28.

[9] Butt, J. R., "A study of morphing wing effectiveness in fighter aircraft using exergy analysis and global optimization techniques," Ph.D. thesis, Virginia Polytechnic Institute and State University, 2005.

[10] Woods, B. K., Bilgen, O., and Friswell, M. I., "Wind tunnel testing of the fish bone active camber morphing concept," *Journal of Intelligent Material Systems and Structures*, Vol. 25, No. 7, 2014, pp. 772–785.

[11] Rivero, A. E., Weaver, P. M., Cooper, J. E., and Woods, B. K., "Parametric structural modelling of fish bone active camber morphing aerofoils," *Journal of Intelligent Material Systems and Structures*, Vol. 29, No. 9, 2018, pp. 2008–2026.

[12] Murugan, M. S., Woods, B. K., and Friswll, M., "Morping helicopter rotor blade with curvilinear fiber composites," 2012.

[13] Beaverstock, C. S., Woods, B. K. S., Fincham, J. H. S.-M., and Friswell, M. I., "Performance Comparison between Optimised Camber and Span for a Morphing Wing," *Aerospace*, Vol. 2, No. 3, 2015, pp. 524–554.

[14] Woods, B. K., Bilgen, O., and Friswell, M. I., "Wind tunnel testing of the fish bone active camber morphing concept," *Journal of Intelligent Material Systems and Structures*, Vol. 25, No. 7, 2014, pp. 772–785.

[15] Brigido-González, J. D., Burrow, S. G., and Woods, B. K., "Switchable stiffness morphing aerostructures based on granular jamming," *Journal of Intelligent Material Systems and Structures*, Vol. 30, No. 17, 2019, pp. 2581–2594.

[16] Liu, A. J., and Nagel, S. R., "Nonlinear dynamics: Jamming is not just cool any more," *Nature*, Vol. 396, No. 6706, 1998, p. 21.

[17] Bi, D., Zhang, J., Chakraborty, B., and Behringer, R. P., "Jamming by shear," *Nature*, Vol. 480, No. 7377, 2011, p. 355.

[18] Behringer, R. P., "Jamming in granular materials," *Comptes Rendus Physique*, Vol. 16, No. 1, 2015, pp. 10–25.

[19] Jaeger, H. M., "Celebrating soft matter's 10th anniversary: Toward jamming by design," *Soft matter*, Vol. 11, No. 1, 2015, pp. 12–27.

[20] Svetel, I., "Prof. Ivan Petrovic, PhD, M. Arch (1932-2000)," *Automation in Construction*, Vol. 2, No. 11, 2002, pp. 129–130.

[21] Loeve, A. J., van de Ven, O. S., Vogel, J. G., Breedveld, P., and Dankelman, J., "Vacuum packed particles as flexible endoscope guides with controllable rigidity," *Granular matter*, Vol. 12, No. 6, 2010, pp. 543–554.

[22] Cheng, N. G., Lobovsky, M. B., Keating, S. J., Setapen, A. M., Gero, K. I., Hosoi, A. E., and Iagnemma, K. D., "Design and analysis of a robust, low-cost, highly articulated manipulator enabled by jamming of granular media," *2012 IEEE International Conference on Robotics and Automation*, IEEE, 2012, pp. 4328–4333.

[23] Huijben, F., "Vacuumatics: 3D formwork systems: Investigations of the structural and morphological nature of vacuumatic structures so as to be used as semi-rigid formwork systems for producing'free forms' and customised surface textures in concrete for architectural applications," 2014.

[24] Naaman, A. E., *Prestressed concrete analysis and design: Fundamentals*, McGraw-Hill New York, 1982.

[25] Arthur, N., "Nilson Arthur H,(1987)"Design of prestressed concrete"," , 1987.

[26] Menn, C., *Prestressed concrete bridges*, Birkhäuser, 2012.

[27] Nawy, E. G., *Prestressed concrete. A fundamental approach*, Second Edition, 1996.

[28] Shih, M.-H., and Sung, W.-P., "Application of digital image correlation method for analysing crack variation of reinforced concrete beams," *Sadhana*, Vol. 38, No. 4, 2013, pp. 723–741.

[29] Wolff, M. F., Salikov, V., Antonyuk, S., Heinrich, S., and Schneider, G. A., "Three-dimensional discrete element modeling of micromechanical bending tests of ceramic–polymer composite materials," *Powder technology*, Vol. 248, 2013, pp. 77–83.